ORIGINAL ARTICLE

Pulsatile Flow Interaction between Aorta and Pulmonary Artery

Takahisa Yamamoto[1], Takumi Ichihashi[1], Shu Ishida[1], Etsuji Nomura[1], Mohamad Ikhwan Kori[2], Kahar Osman[2]

[1] Departiment of Mechanical Engineering, National Institute of Technology, Gifu College, 2236-2 Kamimakuwa, Motosu 501-0495, Japan
[2] IJN-UTM Cardiovascular Engineering Centre, Universiti Teknologi Malaysia, 81310 UTM Johor Bahru, Johor, Malaysia

ABSTRACT

Introduction: Hypoplastic left heart patients have significant blood flow unbalance in the cardiovascular system; excess blood flows from the right ventricles to the lung. Patent Ductus Arteriosus (PDA) stenting prevents excess blood flow and shunts the blood flow to the aorta through PDA without conventional heart surgeries. On the other hand, past clinical researches report that PDA stenting can bring on thrombosis around ductus arteriosus. This study elucidated the hemodynamics of the aorta-pulmonary artery system by using three patient-specific morphological data, experimentally and numerically. **Methods:** This study carried out Particle Image Velocimetry (PIV) measurement and Computational Fluid Dynamics (CFD) analysis for three patient-specific models. **Results:** The experimental and numerical analysis clarified transient hemodynamics in the aorta-pulmonary artery system; pulmonary blood flow was shunt to the aorta at the peak systole and diastole. Q-criterion, which indicates both the second-order invariant of turbulence flow and the structure's characteristics, was generated in the PDA at the same period. **Conclusion:** This study found the influence of PDA morphology on transient hemodynamics; the highest Q-criterion in the PDA is 600 [s-2]; on the contrary, the lowest case is around 200 [s-2]. These flow characteristics are essential factors in thrombus formation in PDA.

Keywords: Computer Fluid Dynamics Simulation, Hemodynamics, Aorta-Pulmonary Artery system

Corresponding Author:
Takahisa Yamamoto, PhD
Email: ytaka@gifu-nct.ac.jp,
Tel:+81-58-320-1336

INTRODUCTION

Hypoplastic left heart syndrome is a congenital heart disease caused by incorrect development of the left system (1, 2). During pregnancy, the patent ductus arteriosus (PDA) maintains the patient's blood flow balance in the cardiovascular system; the excess blood flow from the right ventricle to the pulmonary artery is shunted to the aorta via PDA. After birth, the ductus arteriosus closes spontaneously.All of the blood flow from the right ventricle flow into the pulmonary artery. Consequently, blood flow to the lungs significantly increase. Some operations are required to save the child patient; the Norwood procedure and the Bidirectional Glenn procedure. Finally, the Fontan procedure is performed to improve cardiopulmonary function. Without surgery, the hypoplastic left heart syndrome is deadly, usually within a few weekds of life. PDA stenting is recently performed instead of the Norwood procedure and the Bidirectional Glenn procedure (3, 4, 5). This operation inserts a stent into the PDA to open the blood vessel. The feature is a minimally invasive technique and avoids the needed cardiopulmonary bypass and circulatory arrest. Although the advances in interventional trans-catheter stenting techniques in the congenital heart have reduced the numbers of mortality and morbidity on neonates, many complications are reported after the stent insertion, such as acute stent thrombosis, PDA spasm, stent migration, pulmonary hypertension, and protrusion (6, 7, 8). The detailed interaction mechanisms of cardiac blood flows in the aorta and the pulmonary artery through the PDA are not studied. It is necessary to reveal the blood flow characteristics in the aorta-pulmonary artery system at the state of the PDA stenting. This study elucidates the hemodynamics of the aorta-pulmonary artery system using both particle image velocimetry (PIV) measurement and computational fluid dynamics (CFD) analysis.

MATERIALS AND METHODS

Case data

This study has used three patient-originated aorta-pulmonary artery models developed in our previous study (9). Figure 1 shows the schematic drawings of the models. The models can be categorized by the PDA origin at the aorta and the insertion point at the pulmonary artery; the PDA origins are categolized by ascending aorta (AS), transverse aorta (TR), and descending aorta

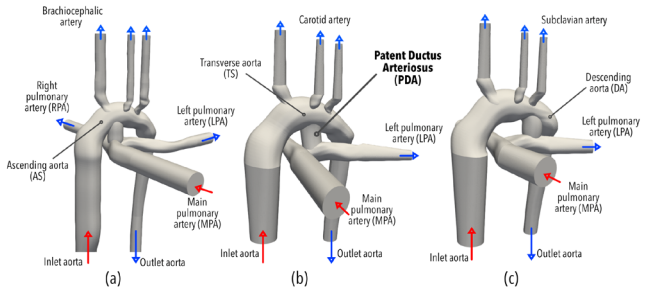

Figure 1: Schematic drawing of the aorta-pulmonary artery models; (a) ASMPA: the PDA origin is at the ascending aorta (AS) and the insertion at the main pulmonary artery (MPA), (b) TRLPA: the PDA origin is at the transverse aorta (TR) and the insetion at the left pulmonary artery (LPA), and (c) DSLPA: the PDA origin is at the descending aorta (DS) and the insetion at the left pulmonary artery (LPA).

(DS), while the insertion point is characterized by the main pulmonary artery (MPA), left pulmonary aorta (LPA), and right pulmonary aorta (LPA). The diameters of AS, DS and LPA/RPA are 13 mm, 11 mm and 6 mm, respectively. Brachiocephalic, subclavian, and carotid arteries diameters have a diameter of 3 mm, PDA of 6 mm in each model.

Numerical model

This study has conducted CFD analysis through the CFD library "OpenFOAM ver.8" to estimate pulsatile flow's influence on the interaction between the aorta and pulmonary artery blood flows. LES (Large Eddy Simulation) turbulent model with WALE (Wall-Adappting Local Eddy-viscosity) sub-grid scale model was employed in this study (10). In LES model, the filtered continuity and Navier-Stokes equations are as follows;

$$\frac{\partial \overline{u_i}}{\partial x_i} = 0 \quad (1)$$

$$\frac{\partial \overline{u_i}}{\partial t} + \overline{u_i}\frac{\partial \overline{u_i}}{\partial x_j} = -\frac{1}{\rho}\frac{\partial \bar{p}}{\partial x_i} + \frac{\partial}{\partial x_i}\left(-T_{ij} - 2\nu S_{ij}\right) \quad (2)$$

where

$$T_{ij} = \overline{u_i u_j} - \overline{u_i}\,\overline{u_j} \quad (3)$$

is the subgrid scale tensor. Applying an eddy-visocosity assumption to the tensor, then the tensor is evaluated by

$$T_{ij} - \frac{1}{3}T_{kk}S_{ij} = 2\nu_t \overline{s_{ij}} \quad (4)$$

Here

$$S_{ij} = \frac{1}{2}\left(\frac{\partial \overline{u_i}}{\partial x_j} + \frac{\partial \overline{u_j}}{\partial x_i}\right) \quad (5)$$

is the deformation tensor of the resolved field. The eddy-viscosity of the WALE model is calculated by

$$\nu_t = (c_w \Delta)^2 \cdot \frac{\left(s_{ij}^d s_{ij}^d\right)^{3/2}}{\left(\overline{S_{ij}S_{ij}}\right)^{\frac{5}{2}} + \left(s_{ij}^d s_{ij}^d\right)^{\frac{5}{4}}} \quad (6)$$

where

$$S_{ij}^d = \frac{1}{2}\left(\overline{g_{ij}^2} + \overline{g_{ji}^2}\right) - \frac{1}{3}\delta_{ij}g_{kk}^2 \quad (7)$$

$$g_{ij} = \frac{\partial \overline{u_i}}{\partial x_j} \quad (8)$$

$(\overline{g_{ij}})$ is the velocity gradient tensor, and S_{ij}^d is the traceless symmetric part of the square of the velocity gradient. c_w is the model constant. This study set c_w=0.325. The blood properties were set at 1050 kg/m3 for the density, and 0.012171 Pa s for the dynamic viscosity. Pulsatile velocity profiles, shown in Fig.2, was aplied at the aorta and main pulmonary artery based on the result obtained from Pennati et al (11). This study discretized the governing equations mentioned above using the finite volume method. The analysis used an unstructured computational mesh consisting of tetra with prism mesh on wall boundaries. The total numbers of meshes in each case are more than 1.5 million. As for the discretization scheme, this study adopted a second-order upwind scheme on advection terms, a second-order central differential scheme on diffusion terms, and an Euler implicit scheme on time terms. The discretized equations are solved by using both Preconditioned conjugate gradient (PCG) solver and preconditioned bi-conjugate gradient stabilized (PBiCGstab) solver.

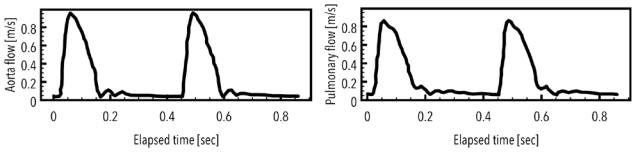

Figure 2: Pulsatile inflow profiles for (a) aorta and (b) main pulmonary artery

Particle Image Velocimetry

PIV measurement is a calculation method for unsteady and instantaneous flow characteristics using image analysis techniques. This measurement method visualizes fluid motion using tracer particles in fluid flow and then estimates the particle velocity numerically using digital image processing (12, 13). The PIV apparatus in this study shows in Fig. 3. It consists of a high-speed camera (DITECT D71, 800fps), a laser light source (DITECT 3W green laser), tracer particles (DANTEC PSP 20μm), and aqueous glycerol aqueous solution as working fluid. A living-body model of the aorta-pulmonary artery system was made from patient-specific 3-D CT data, as shown in Fig. 4. It was originated from the ASMPA model shown in Fig. 1 (a). It was made from silicon rubber, and it is twice as large as the actual body scale. The red rectangle in Fig. 4 is the imaging object region. Liquid delivery pumps connected with both aorta and pulmonary artery inlets of the model. During the PIV measurement, these flow rates were set at 0.650 (L/min) and 0.823 (L/min), respectively.

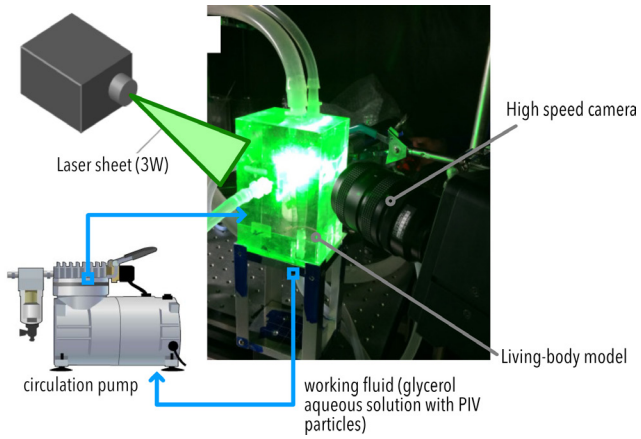

Figure 3: Schematic drawing of Particle-Image-Velocimetry system

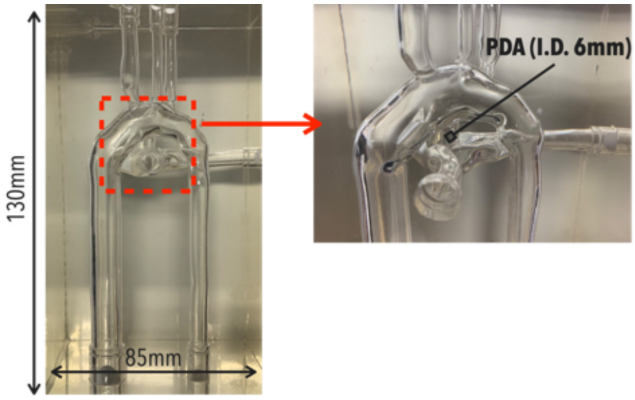

Figure 4: ASMPA Living model of Aorta-Pulmonary artery system for Particle-Image-Velocimetry measurement

RESULTS

Velocity characteristics in constant flow condition (Result of PIV measurement)

This study conducted a PIV measurement using the living-body model under constant flow rate conditions. Fig. 5 shows PIV measurement results, especially Fig.5(c) is the time-averaged z-direction (axial) velocity compared with CFD analysis. The low-velocity region forms both inside the PDA and the junction of the PDA and the aorta. Circulation flow inside the PDA, namely up-flow and down-flow, is also found in this region. These characteristics indicate the bloow flows interaction between the aorta and pulmonary artery. The CFD analysis shows qualitatively good agreement with PIV measurement, although CFD analysis shows quantitative differences with PIV measurements. The differences were caused by discrepancies in outlet boundary conditions in CFD analysis. There is still room for consideration; this study proceeds with discussing pulsatile flow characteristics in the PDA using CFD analysis in the following sections.

Hemodynamics in pulsatile flow condition (Result of CFD)

Figure 6 shows velocity contours on the coronal plane of the PDA before systole, at peak systole, and diastole; the results of the three models show completely different blood flow transient characteristics. In the ASMPA before systole (t=0.47s), there are low-velocity regions inside PDA; blood flow re-balance, where blood flow from the pulmonary artery to the aorta, does not occur at this period, as shown in Fig.6(a). Blood flow from the aorta to pulmonary artery slightly appears at the peak systole (t=0.52s), as shown in Fig.6(b). Subsequently, vertical circulation flow is observed inside PDA at the diastole (t=0.60s), as shown in Fig.6(c). In TRLPA, blood

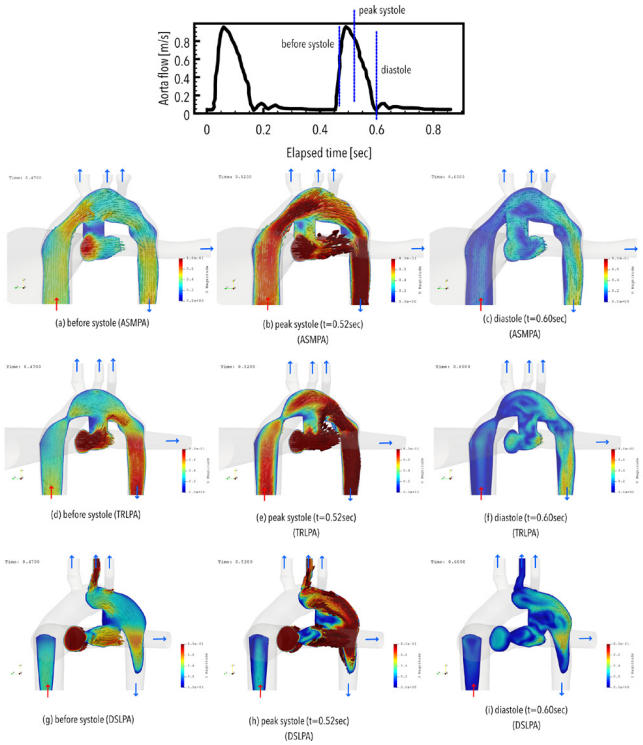

Figure 6: Velocity contours on the coronal plane of the PDA before systole, at peak systole, and at diastole

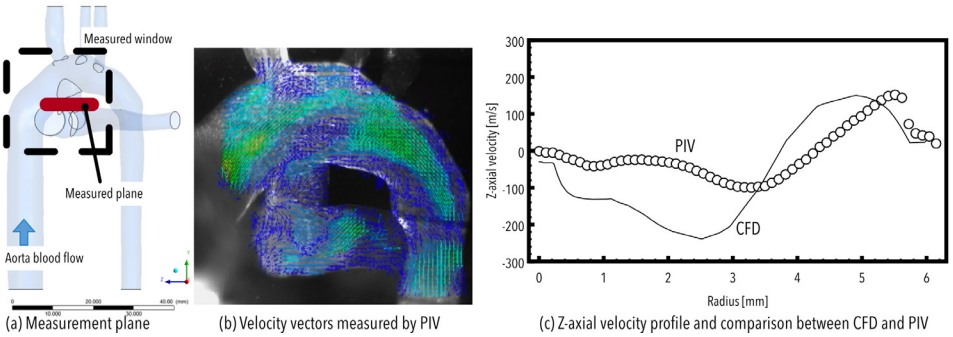

Figure 5: Result of PIV measurement inside PDA and comparison with CFD; (a) the location of measurement section, (b) instantaneous velocity vectors, and (c) time-averaged z-direction (axial) velocity inside PDA comparing with CFD analysis

flow from the pulmonary artery to the aorta is observed before and at the systole, as shown in Figs.6(d) and 6(e). On the other hand, in DSLPA, significant blood flow interaction between the aorta and the pulmonary artery does not appear during the systole and the diastole, as shown in Figs.6(g)-6(i).

DISCUSSION

This study calculated Q-criterion, the second-order invariant of turbulence flow, and indicates the vortex structure's characteristics in the flow to understand the PDA's pulsatile flow characteristics more deeply. The Q-criterion is evaluated as,

$$Q = \frac{1}{2}(W_{ij}W_{ji}) \quad (9),$$

where,

$$W_{ij} = \frac{\partial u_j}{\partial x_i} \quad (10),$$

is the velocity gradient.

As shown in Fig. 7, the main pulmonary artery's vortices transfer to the aorta via the PDA at the peak systole in all cases. In the case of ASMPA, most of the vortices in the PDA disappear at the diastole, as shown in Fig.7(c). Then the highest Q-criterion in the PDA is 212 [s^{-2}]. On the other hand, vortices still continue to be generated at the diastole in both TRLPA and DSLPA, as shown in Figs.7(f) and 7(i). In addition, the highest Q-criterions in both cases are above 600 [s^{-2}]. The PDA stent is inserted into the PDA to enlarge the tiny blood vessel in a practical situation. As calculation results of velocity and vortex, the stent insertion to both TRLPA and DSLPA will induce and encourage the mixing vortices in the low-velocity regions, consequently suppressing the thrombus formation within the aorta-pulmonary artery system. The design of the PDA stent that persuades turbulence is to be important in stent development. The previous study had only carried out steady flow analysis, revealing velocity contours in the PDA system (9, 14-16). This study had analyzed the transient flow characteristics and vortices formation and dissipation characteristics in the aorta-pulmonary artery system. Furthermore, this study clarified the influence of the blood vessel morphology on the blood flow and vortex characteristics. These results give us detailed information about re-balance characteristics, which is a great advantage of this study.

CONCLUSION

This study performed CFD analysis and PIV measurement for blood flow characteristics in the aorta-pulmonary artery system. This study found that the circulation flow is formed in the PDA from the PIV measurement. CFD analysis under the same flow condition with PIV measurements gave qualitatively similar characteristics. In the CFD analysis under pulsatile flow conditions, this study found the influence of aorta, PDA, and pulmonary

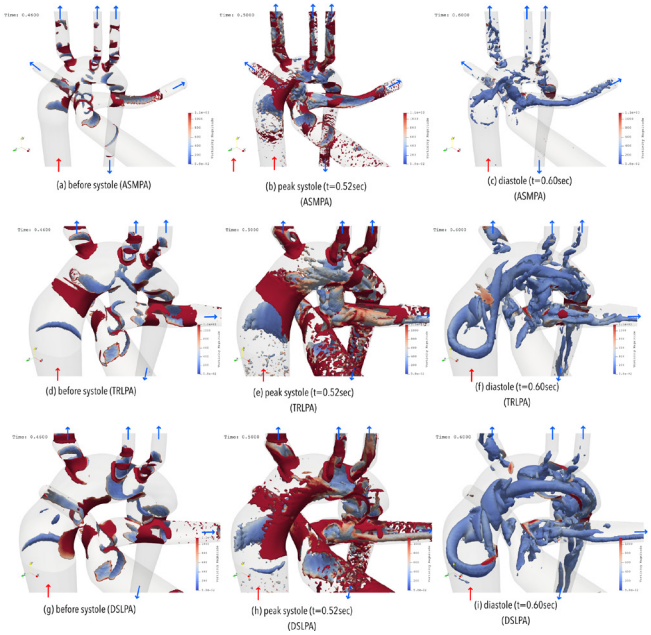

Figure 7: Visualization of generation and dissipation of vortices; contour surface of the Q-criterion before systole, at peak systole, and at diastole

artery morphologies on the blood flow characteristics in the system; blood flow from the pulmonary artery to the aorta is formed, and the Q-criterion vortices generated during systole and diastole periods in two of the three cases. Since the low-velocity and low Q-criterion vortices regions will be significant to the thrombus formation and the stent will be induced turbulence in the regions, stent design will be essential to suppress the thrombus formation.

ACKNOWLEDGEMENT

This work was financially supported by the JSPS KAKENHI Grant Number 19K04181.

REFERENCES

1. Zahka K, Spector M, Hanisch D. Hypoprastic Left-Heart Syndrome Norwood Operation, Transplantation, or Compassionate Care. Clinics in Perinatology. 1993;20(1):145-154.
2. Newburger J. Triedman J. Trends in Congenital Heart Disease. Circulation. 2016;133(25): 2716-2733.
3. Alwi M, Choo KK, Latiff HA, Kandavello G, Saimon H, Mulyadi MD. Initial Results and Medium-Term Follow-Up of Stent Implantation of Patent Ductus Arteriosus in Duct-Dependent Pulmonary Circulation. J. American College of Cardiology. 2004;44(2):438-445.
4. Boucek, M., Mashburn, C. & Chan, K., 2005. Ductal Anatomy: a Determinant of Successful Stenting in Hypoplastic Left Heart Syndrome. PEDIATR CARDIOL, 26(2), pp. 200-205.
5. Egan, M. et al., 2011. Histopathologic Evaluation

of Patent Ductus Arteriosus Stents After Hybrid Stage I Palliation. Pediatric Cardiology, 32(1), pp. 413-417.

6. Galantowicz, M., Cheatham, J., Phillips, A. & Cua, C., 2008. Hybrid approach for hypoplastic left heart syndrome: intermediate results after the learning curve. Ann Thorac Surg., 85(6), pp. 2063-2070.
7. Alwi, M., Choo, K. & Radzi, N., 2011. oncomitant stenting of the patent ductus arteriosus and radiofrequency valvotomy in pulmonary atresia with intact ventricular septum and intermediate right ventricle: Early in-hospital and medium-term outcomes. The Journal of Thoracic and Cardiovascular Surgery, Volume 141, pp. 1355-1361.
8. Alwi, M., 2008. Stenting the ductus arteriosus: Case selection, technique and possible complications. Ann Pediatr Cardiol., 1(1), pp. 38-45.
9. Ikhwan Kori, M., Osman, K. & Taib, I., 2017. Hemodynamic prediction in patent ductus arteriosus morphologies. ARPN J Engineering and Applied Science, 12(10), pp. 3156-3160.
10. Nicoud, F. & Ducros, F., 1999. Subgrid-Scale Stress Modelling Based on the Square of the Velocity Gradient Tensor. Flow, Turbulence and Combustion, 62(1), pp. 183-200.
11. Pennati, G., Belloti, M. & Fumero, R., 1997. Mathematical modeling of the human foetal cardiovascular system based on doppler ultarasound data. Medical Engineering and Physics, 19(4), pp. 327-335.
12. Busen, et al., 2015. In vitro flow investigations in the aortic arch during cardiopulmonary bypass with stereo-PIV. J Biomech., 48(10), pp. 2005-2011.
13. Murai, Y., Ido, T., Ishikawa, M. & Yamamoto, F., 1998. Development of the Post-Processing Method for PIV Measurement Result Using Computational Fluid Dynamics Procedure. Trans JSME Series B, 64(626), pp. 3249-3256.
14. Boumpouli, M., Danton, M., Gourlay T., Kazakidi, A., 2020. OP7 Understanding the blood flow in realistic and idealised models of the pulmonary bifurcation. Heart Journal, 106(A3-A4).
15. Lopes, D., Puga, H., Texieira, J. Lima, R., 2020. Blood flow simulations in patient-specific geometries of the carotid artery: A systematic review. J. Biomechanics, 111(9), pp.1-17.
16. Jamal, T., Wang, H., Walters, D.K., 2018. LES and Hybrid RANS-LES simulation of a Pulsating Channel Flow. Proceedings of ASME Int. Mech. Eng. Congress and Exposition, 7, Paper No. IMECE2018-87990.